CONNECTING MOTORS AND MEMBRANES:
A QUANTITATIVE INVESTIGATION OF DYNEIN PATHWAY COMPONENTS
AND *IN VITRO* CHARACTERIZATION OF THE NUM1 COILED COIL DOMAIN

A Thesis Presented

by

BRYAN JOSPEH ST. GERMAIN

Submitted to the Graduate School of the
University of Massachusetts Amherst in partial fulfillment
of the requirements for the degree of

MASTER OF SCIENCE

September 2011

Molecular and Cellular Biology

CONNECTING MOTORS AND MEMBRANES:
A QUANTITATIVE INVESTIGATION OF DYNEIN PATHWAY COMPONENTS
AND *IN VITRO* CHARACTERIZATION OF THE NUM1 COILED COIL DOMAIN

A Thesis Presented

by

BRYAN JOSEPH ST. GERMAIN

Approved as to style and content by:

_____

Wei-Lih Lee, Chair

_____

Patricia Wadsworth, Member

_____

Thomas Maresca, Member

_____

Barbara Osborne, Department Head

Molecular and Cellular Biology

I would like to dedicate this thesis in loving memory of Virginia Bush, the greatest mother/grandmother to ever see the sun shine. I miss you terribly and none of my accomplishments would have been possible without your love and guidance.

ABSTRACT

CONNECTING MOTORS AND MEMBRANES:
A QUANTITATIVE INVESTIGATION OF DYNEIN PATHWAY COMPONENTS
AND *IN VITRO* CHARACTERIZATION OF THE NUM1 COILED COIL DOMAIN

SEPTEMBER 2011

BRYAN JOSEPH ST. GERMAIN, B.S., UNIVERSITY OF MASSACUSETTS

AMHERST

M.S., UNIVERSITY OF MASSACHUSETTS AMHERST

Directed by: Professor Wei-Lih Lee

In the budding yeast, *Saccharomyces Cerevisiae,* dynein, a minus-end directed motor, is involved in nuclear migration and proper orientation of the mitotic spindle during mitosis. Our lab has developed a model that involves the loading of cytoplasmic dynein onto the plus-end of astral microtubules through interactions with Pac1/LIS1 and Bik1/CLIP-170. Dynein is then delivered to the cell cortex and anchored through a cortical receptor protein, Num1. Num1 is a 313KDa protein that localizes to the cell cortex and is an essential component of dynein mediated nuclear migration.

Using quantitative fluorescence techniques I was able to create a molecular inventory of various dynein pathway components. Our results revealed Dyn1, dynein heavy chain, and Pac1/LIS1 associate at the plus end in a 1:1 ratio. Additionally we found that dynein and dynactin associate in a 3:1 ratio

at the plus ends and a 2:1 ratio at the cortex. Interestingly, we found that over expression of Pac1/LIS1 augments cortical dynein activity while maintaining the dynein to dynactin ratio and this activity is separate from loss of She1, a negative regulator of dynein-dynactin interaction, which results in a 1:1 ratio of dynein-dynactin at the plus-ends, as well as, the cortex. Our results uncover molecular ratios that enable us to create more defined and detailed model of the dynein pathway.

To elucidate how Num1 attaches dynein to the cortex we created truncations of the Num1 protein. We were able to determine that two coiled-coil (CC) domains in the N-terminus of Num1 are responsible for bright foci formation on the cortex. Cells without these bright foci exhibit a binucleate phenotype similar to that of *dyn1Δ* implicating that these bright foci are required for the proper function of Num1 in the dynein pathway.

To test the hypothesis that the CC is capable of mediated bright patch assembly through self-association I purified a recombinant CC domain and performed gel filtration analysis, as well as, equilibrium sedimentation.   I was able to determine that the CC domain exists as a dimer in solution. However, the mechanism of CC self-assembly may involve a requisite of targeting the CC to the cortex first.

TABLE OF CONTENTS

Page

LIST OF FIGURES

CHAPTER 1

INTRODUCTION

During mitosis the mitotic spindle must be oriented properly in order for the chromosomes to be properly segregated into each daughter cell. The migration of the mitotic spindle is believed to occur via interactions between the cell cortex and astral microtubules projecting from the microtubule-organizing center. Numerous studies in various organisms including *C. elegans* (Gönczy et al. 1999)*, D. melanogaster* (Ghosh-Roy et al. 2004)*, A. nidulans* (Han et al. 2001) and the budding yeast *S. Cerevisiae* (Heil-Chapdelaine 2001, Bloom et al. 2001, Lee et al. 2005) have indicated that cytoplasmic dynein, a minus-end directed motor, is essential for the interaction between astral microtubules and the cell cortex.

How cytoplasmic dynein is attached at the cell membrane is not fully understood in mammalian systems. In *C. elegans,* Lin-5, a protein that associates with Ga proteins (GOA-1 and GPA-16) and their regulators GPR-1 and GPR-2, has been observed co-immunoprecipitating with dynein light chain (van der Voet, 2009), linking dynein to cortical membrane. Recent work by Schmoranzer et al. (2009) has demonstrated the polarity protein Par3 interacts through its N-terminal PDZ1 domain with dynein intermediate chain 2 during centrosome centration. However, more work must be done to characterize this newly found interaction. Budding yeast is an excellent system to explore

dynein's mitotic function because it is a non-essential protein for nuclear migration. Therefore, elucidation of the mechanism that attaches cytoplasmic dynein to the cell cortex in budding yeast may provide insight into conserved mechanisms of dynein-mediated spindle positioning in other organisms.

In yeast, the site of cytokinesis is at the bud neck, meaning the nucleus must be properly translocated from the mother cell into the incipient bud for proper segregation of the chromosomes. Failure of cells to properly orient the nucleus during mitosis eventually results in a delay in cell cycle progression and improper cell division; this consequentially leaves one cell with no nuclei and one cell with two nuclei, known as a binucleate phenotype.

Previously it has been shown that two separate but overlapping pathways facilitate movement of the nucleus into the bud cell. *KAR9* and dynein function in redundant pathways during nuclear migration, however they act through different components. The *KAR9* pathway involved the cortical protein Kar9 that uses a capture shrinkage method to pull the spindle into the daughter cell (Beach, 2000). In the dynein-dependent pathway, dynein is loaded onto the plus end of astral microtubules that project through the bud neck into the nascent bud. Dynein is then hypothesized to offload at the plasma membrane when the plus ends of the astral microtubules come in contact with the cell cortex. Dynein, now attached to cortex, pulls the bound astral microtubule and walks towards the spindle pole in a minus-end directed manner (Bloom, 2001; Lee, 2005). This pulling force causes sliding of the astral microtubule along the cortex and subsequent translocation of the nucleus into the newly budded cell.

The nuclear migration protein Num1 localizes to discrete puncta at the cell cortex (Heil-Chapdelaine, 2000). Num1 contains a C-terminal Pleckstrin Homology (PH) domain that diates interactions with PI(4,5)P$_2$ lipids (Tang et al. 2009). It has been shown that *num1Δ* strains are synthetic lethal when combined with a *kar9Δ* deletion, placing *NUM1* in the dynein dependent pathway. Moreover *num1Δ* cells exhibit a binucleate phenotype similar to that seen in cells lacking the dynein heavy chain *dyn1Δ* (Heil-Chapdelaine, 2001). Dyn1 has been observed colocalizing with patches of Num1, further implicating Num1 as the cortical receptor protein in the offloading model. Moreover, domain analysis of Dyn1 showed that the C-terminal motor domain of Dyn1 targets the heavy chain to astral microtubule plus ends in a Pac1 and Bik1-dependent manner, and the N-terminal tail domain of Dyn1 is required for the attachment the heavy chain to Num1 at the cell cortex (Markus et al 2009).

CHAPTER 2

FUNCTIONAL ANALYSIS OF DOMAINS IN NUM1 THAT AFFECT THE DYNEIN PATHWAY

Introduction

To begin elucidating Num1 domain function we constructed various truncations of the NUM1 gene to dissect the function of each domain in the dynein pathway. Truncations were also labeled with GFP and tagged at the chromosome to detect any changes in the localization of Num1. Budding yeast with a defective dynein pathway exhibit a misoriented spindle, which upon completion of mitosis, results in a binucleate phenotype. Using the cold binucleate assay we were able to determine which domains in Num1 are necessary and sufficient for proper function of Num1 in the dynein pathway.

Cold Binucleate Assay

My analysis of Num1 truncations revealed two domains that are required for the proper function of Num1 in the dynein dependent pathway. The first is the aforementioned PH domain, and the second is a domain that lies in the N-terminus (1-303aa) of the protein. The coiled-coil region is predicted by PAIRCOIL2 to contain two coiled-coil domains, CC1 (Δ104-187aa) or CC2 (Δ214-290aa), connected by a short-linking sequence.

I found that cells expressing a Num1 fragment lacking either the PH domain or the CC domains had a similar binucleate phenotype as *num1∆, ~20%* (Figure 1). My results indicate that the CC domains as well as the PH domain are required for Num1's role in spindle positioning. To test whether these domains were sufficient for Num1 function we assayed a fusion protein containing the CC domains attached to the PH domain. We found that this fusion was able to rescue the WT dynein pathway function, thus proving that the CC and PH domains are sufficient for the proper function of Num1 in spindle positioning.

Further analysis of the Num1 truncations shows that deleting the CC1 resulted in a slightly less dramatic binucleate phenotype than deletion of both coiled-coil domains. Notably, cells expressing the ∆CC1-GFP construct also exhibited an inability to form bright foci of Num1 at the cortex when compared to WT cells, resulting in foci 25% as bright as WT cells (Figure 3). No cortical foci were observed in cells expressing ∆CC2 (Figure 2). Previous studies in our lab have shown the PH domain tagged with GFP localizes to the cell cortex as dim foci and heavily to the bud neck (ref). However, when both CC domains were fused to either a CAAX motif or the PH domain of Num1 the fusion was able to form bright foci at the cell cortex (Figure 2). These results support that the CC domain is sufficient for bright patch assembly of Num1 at the cortex.

Discussion

Functional analysis of the domains in Num1 revealed that the CC domains and the PH domain are required for the proper targeting of the protein to the cell cortex, and these domains are sufficient to rescue WT dynein pathway function of Num1. Additional investigation revealed that the deletion of the first CC domain resulted in a loss fluorescence intensity at the cell cortex but dim patches were still visible. Deletion of the second CC domain resulted in no foci likely due to a destabilization of the protein. Loss of these bright foci in cells expressing ΔCC1 corresponded to a severe binucleate phenotype, though not as severe as a *num1Δ* strain. These data support a model that may link the formation of these bright patches to dynein pathway function. To elucidate the mechanism of patch assembly and the CC domains' role in the dynein pathway we constructed plasmids to express the CC domains for biochemical analysis.
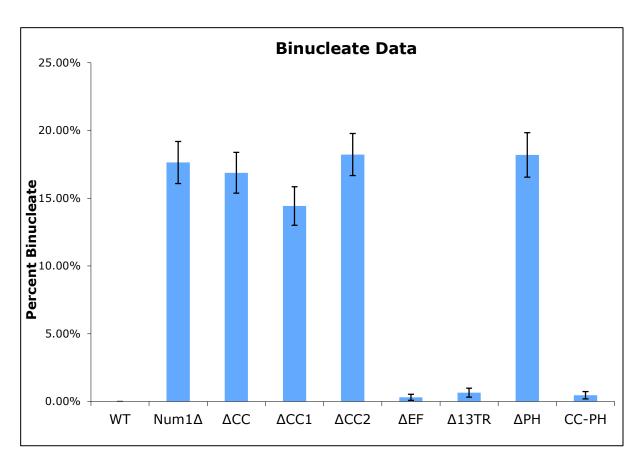
Figure 2.1: Binucleate data in Num1 truncations. Cells were grown overnight in 12° C shaking incubator to mid-log phase. Images were taken and cells were scored for a binucleate phenotype (n>600). Error bars are SE.

Num1-GFP

ΔCC1-GFP

PH-GFP

CC-GFP-PH

CC-GFP

CC-GFP-CAAX
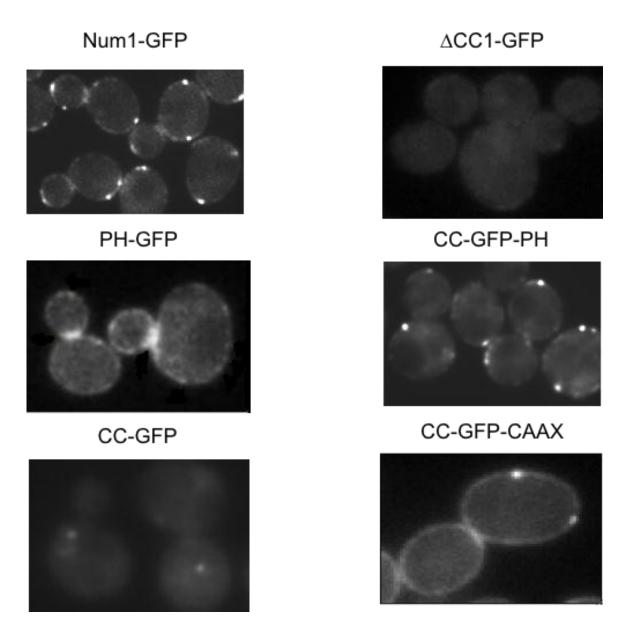
Figure 2.2: Localization of Num1 truncations. Images of cells expressing Num1 truncations tagged with GFP.

A)   B)
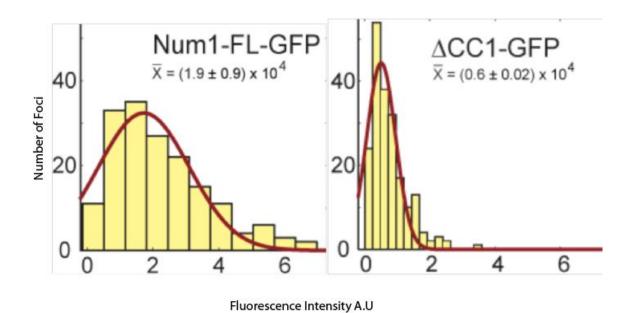
Figure 2.3: Fluorescence Intensity of Num1 foci. Fluorescence intensity of Num1 foci, fit with Gaussian curves, n<173 for both strains. ΔCC1 intensity is 25% of the A.U value obtained from Num1-FL.

CHAPTER 3

**EXPRESSION AND PURIFICATION OF N-TERMINAL
TRUNCATIONS OF NUM1**

Introduction

To biochemically test through gel filtration and analytical

ultracentrifugation (AUC) whether the CC domains' oligomerization is due to self-

association, I constructed plasmids containing fragments of the N-terminal region

of Num1. Once these plasmids were constructed we optimized expression and

purification of the protein to obtain concentrations necessary for gel filtration and

AUC.

Plasmid Construction

To construct the bacterial expression plasmid for purification of S-tagged

coiled-coil domain, a fragment containing a preScission protease cleavage site,

followed by a S-tag, a TEV cleavage site and a IgG-binding site was amplified

from pKW804, using a forward primer flanked with a NotI site followed by a

preScission cleavage site (PCN) and a reverse primer flanked with stop codon

followed by a KpnI site. The PCR fragment was digested with NotI and KpnI and

ligated into similarly digested pSY7 (a gift from Robert Robinson, Institute of

Molecular and Cell Biology, Singapore), generating pBSG01 (pSY7:S-IgG). A

fragment containing Num1 aa 95-303 was then amplified from yeast genomic

DNA using a forward primer flanked with a NcoI site and a reverse primer flanked

with a NotI site. The PCR fragment was then digested with NcoI and NotI and

ligated into similarly digested pBSG01, generating pBSG02 that expresses CC-

S-IgG. Another fragment of Num1 containing 2-315aa was also amplified from

yeast genomic DNA. Using the same ligation strategy designed for the 95-303aa

this fragment was ligated into pSY7, generating pBSG03 that expresses 2-

315aa-S-IgG. Plasmids were transformed into BL21 Rosetta cells for

recombinant protein expression.

Expression and Purification of Num1 Truncations:

 I began my purification using the construct with affinity tags on the N-

terminal end of a Num1 truncation from 1-325aa. This construct was

transformed into BL21 cells and expression was induced for 4 hours with 0.5mM

IPTG. Cells were lysed using 10mL of BugBuster (Novagen) per 250mL culture.

The recombinant protein was purified using a two-step affinity purification

protocol. First, the lysate was bound to Ni-NTA beads, washed three times with

10x bead volume of 1xLEW buffer (50mM NaH_2PO_4, 300mM NaCl, pH 8.0), and

eluted using 250mM imidazole. The eluted protein was then bound to amylose

resin, and washed three times with 10x the bead volume with buffer containing

20mM Tris-HCl pH 7.5, 200mM NaCl, 1mM EDTA, 1mM DTT and 1mM PMSF.

To remove the protein from the beads we added 2μl of PreScision protease

(PCN) and digested the beads for 4 hours at 4˚C. This digestion should, in

theory, cleave CC domain from the MBP-6xHIS tag releasing it from the amylose

beads into the supernatant. Western blot analysis of the PCN digest showed a

significant amount of the tag in my supernatant, along with num1 $_{(1-325aa)}$ (Figure

1A). Attempts to separate the MBP-HIS tag from the protein of interest by

binding the supernatant to amylose resin again were unsuccessful (Figure 1B).

Since we were unable to purify our protein to homogeneity using this strategy, I

redesigned the constructs and created two new plasmids, pBSG02 and pBSG03,

expressing affinity tags at their C-terminus and transformed them into BL21

Rosetta cells for protein expression (See methods above).

To establish the optimal conditions for expression of my new constructs I

performed a temperature screen during inductions at 16˚, 20˚, and 30˚C. I found

inducing our cells at 20˚C for 16 hours gave the most soluble protein (Figure 2A).

Once the proper induction conditions had been established I proceeded to bind

the protein to IgG sepharose beads and was able to remove the CC domains

from the beads by digesting with TEV protease. The TEV protease site cleaves

our construct between the S-tag and the IgG binding domain, effectively

releasing our protein from the beads, while maintaining the S-tag allowing us to

track the CC domain via western blot (Figure 2B).   Now that I was able to attain

high concentrations of our recombinant CC domains we can use gel filtration and

AUC to determine the oligomeric state of our protein.   The methods pertaining to

the purification for gel filtration and AUC can be found in the following chapter.
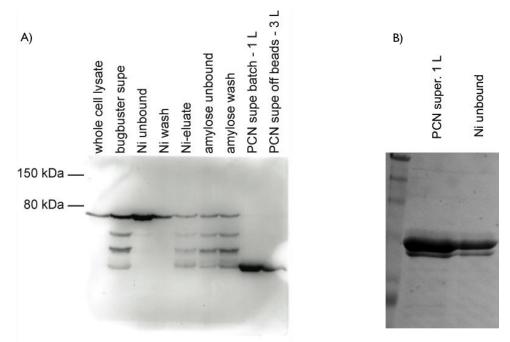
Figure 3.1: Purification of MBP-HIS-CC$_{1-325aa}$ using Ni-NTA and Amylose Resin. A) Western blot analysis using anti-His antibody to track affinity tags throughout the purification. B) Re-binding of PCN digest to Ni-NTA beads in attempt to purify recombinant CC to homogeneity. Unbound lane shows the presence of tag in the unbound fraction.
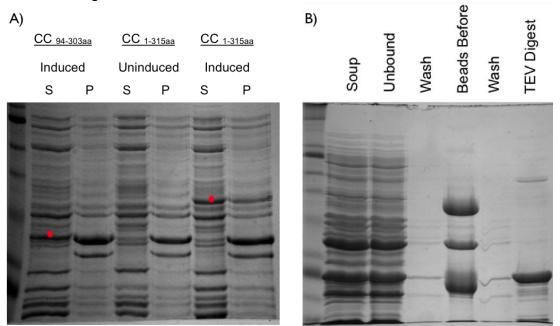
Figure 3.2: Induction and purification of recombinant num1 truncations. A) Gel showing induction of two recombinant CC constructs, 94-303aa and 1-315aa. Cells were induced with 0.5mM IPTG for 16 hours at 20°C. B) Purification of CC$_{94-303aa}$ through binding to IgG sepharose beads and subsequent digest with TEV protease, cleaving the CC-S from the beads.

CHAPTER 4

BIOCHEMICAL CHARACTERIZATION TO DETERMINE THE OLIGOMERIC STATE OF THE CC DOMAINS *IN VITRO*

Introduction

   To test whether the CC domain is capable of forming multimers through self-association we purified protein expressed from our $CC_{95-303aa}$ construct, using the protocol described below, and applied our recombinant protein to a gel filtration column. This technique will allow us to determine the hydrodynamic radius of the native protein in solution, and provide us with information pertaining to the size of our protein. Since gel filtration cannot be used to resolve the molecular weight of a protein we intend to perform analytical ultracentrifugation to determine the molecular weight of the native species. Through the use of these techniques we will not only be able to determine the molecular weight and hydrodynamic radius of our protein but also the multimeric state of our protein in solution.

Gel filtration and sedimentation equilibrium analyses

   To purify CC-S for gel filtration, 4 L of *E. Coli* BL21 Rosetta cells carrying pBSG02 were induced in the presence of 0.5mM IPTG to express CC-S-IgG at 20°C for 16h. Cells were lysed in 64 ml of IgG bind/wash buffer A (150mM NaCl + 20mM Tris-Cl (pH 7.5) + 0.05% Triton X-100 + 1 mM EDTA + 1mM DTT + 1mM PMSF), supplemented with protease inhibitor cocktail (Roche Biochemicals), by vortexing 5 times for 1 min using a bench top vortex mixer after adding 0.1mm glass beads. Cell lysates were cleared by centrifugation at

4°C for 20 minutes. The cleared supernatant was added to 1.5ml of IgG

sepharose beads (6 Fast Flow, GE Healthcare) and incubated at 4°C for 45 min

with gentle rotation. The sepharose beads were then washed 3 times with IgG

bind/wash buffer A. The washed beads were resuspended into 1.2ml of IgG

bind/wash buffer A containing TEV protease and incubated at 16°C for 3h with

rotation. The TEV eluate (CC-S) was applied to a 200ml column of Sephacryl

S200 equilibrated with IgG bind/wash buffer A. Fractions of 2ml were collected

and assayed by western blotting with anti-S-tag and coomassie stained gel. The

S200 column was calibrated with ATP (salt volume) and standard proteins

(Sigma) including blue dextran (MW 2000 kDa, void volume), BSA (MW 66 kDa,

Stoke's radius (Rs) 3.55nm), carbonic anhydrase from bovine erythrocytes (MW

29 kDa, Rs 2.36nm), alcohol dehydrogenase from yeasts (MW 150 kDa, Rs

4.6nm), β-amylase from sweet potato (MW 200 kDa, Rs 5.40nm), and apoferritin

from horse spleen (MW 443 kDa, Rs 6.1nm). The apparent molecular weight of

CC-S was calculated by comparing its Ve/V0 value to the calibration curve. To

calculate the stoke's radius of CC-S, the parameter Kd for each standard protein

was calculated from the expression Kd = (Ve-Vo) / (Vt-Vg-Vo), where Ve =

elution volume of the protein, Vo = void volume, Vt = total volume and Vg =

volume of the gel matrix. The Rs of CC-S was obtained from plot of kd^(1/3)

versus Rs according to (Mainwaring 1969).

CC-S used for analytical ultracentrifugation analysis was similarly purified

from *E. Coli.* cells expressing pBSG02. Briefly, 8 L of *E. Coli.* BL21 Rosetta cells

were lysed in 128 ml of IgG bind/wash buffer B (150 mM NaCl + 20 mM Tris-Cl

(pH 7.5) + 0.05% Triton X-100 + 1 mM EDTA + 0.1 mM TCEP (*tris*(2-carboxyethyl)phosphine) + 1 mM PMSF), supplemented with protease inhibitor cocktail. The cleared lysates was incubated with IgG sepharose beads at 4°C for 45 min, followed by wash with IgG bind/wash buffer B three times and then wash with IgG bind/wash buffer C (150 mM NaCl + 20 mM Tris-Cl (pH 7.5) + 1 mM EDTA + 0.1 mM TCEP (*tris*(2-carboxyethyl)phosphine) + 1 mM PMSF) three times. The washed beads were then digested with TEV protease in buffer C at 16°C for 3h. The TEV eluates were further purified by Sephacryl S200 gel filtration in IgG bind/wash buffer C containing no PMSF. Gel filtration fractions containing CC-S were pooled and concentrated using an Amicon Ultra centrifugal filter with a molecular weight cut-off of 3,000 (Millipore) to approximately 0.6 mg/ml prior to analytical ultracentrifugation analysis. Sedimentation equilibrium experiments were performed with a Beckman Optima XL-I analytical ultracentrifuge by using absorbance optics. A Ti60 4-hole rotor was used with 2-sectored centerpieces. CC-S sample with A_{280} of 0.49 at 280nm was spun at three speeds (14, 000 rpm, 20,000 rpm and 28,000 rpm) at 20°C. A_{280} scans occurred every hour during the spin. Equilibrium data from all speeds were fit as a group using HeteroAnalysis (Version 1.1.0.44 written by J. Cole and J. Lary, University of Connecticut) and the fitting was verified by WinNONLIN (written by J. Lary and D. A. Yphantis, University of Connecticut).

Discussion

To test whether the CC domain is capable self-association I applied the

purified CC$_{(95-303aa)}$ -Stag to a gel filtration column. The protein surprisingly,

based on the elution profile of our standards, eluted with peak fractions

corresponding to ~200kDa molecular weight and a hydrodynamic radius of

5.08nm (Figure 1). The recombinant protein is predicted to have a monomeric

weight of 27.5kDa. There are two possible interpretations from the elution profile

of our recombinant protein. The first is that our protein exists as an octamer in its

native state and is therefore capable of self-association in solution. The other

possibility is that our protein is in fact an elongated structure and possibly does

not exist as a multimeric structure. In an attempt to test the self-association

hypothesis I increased the salt concentration of our buffer to 500mM NaCl in an

attempt to disrupt any electrostatic interactions, however our protein eluted in the

same fraction indicating that either 500mM NaCl was not sufficient to disrupt

intermolecular interactions or our protein does not oligomerize to a higher order

structure.

Due to the inconclusive result from gel filtration, I analyzed the CC$_{(95-303aa)}$

using sedimentation equilibrium analysis to determine the actual molecular

weight of our species in solution. Analysis of the AUC data revealed that the

molecular weight of our protein was 55.6kDa, proving that the CC$_{(95-303aa)}$ forms a

dimer in solution and is incapable of forming a higher order structure in solution
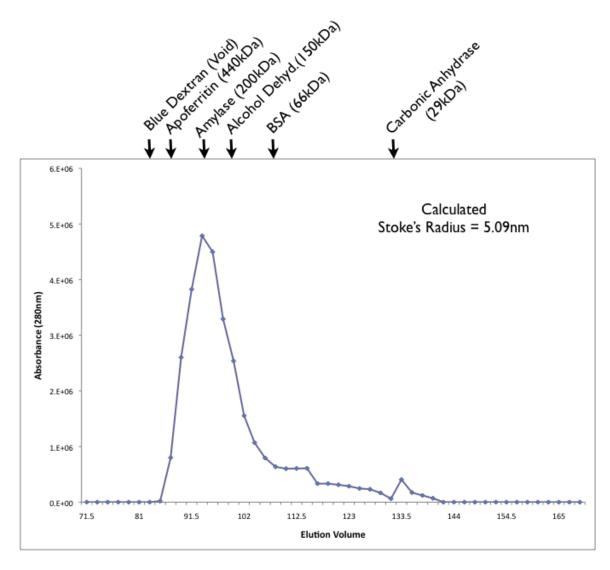
in vitro.

17

Figure 4.1: Gel filtration elution profile of CC-Stag. Absorbance$_{280}$ readings in each fraction collected from gel filtration. Arrows indicate the peak intensity from each molecular weight standard used. Stokes radius was calculated using methods described above.

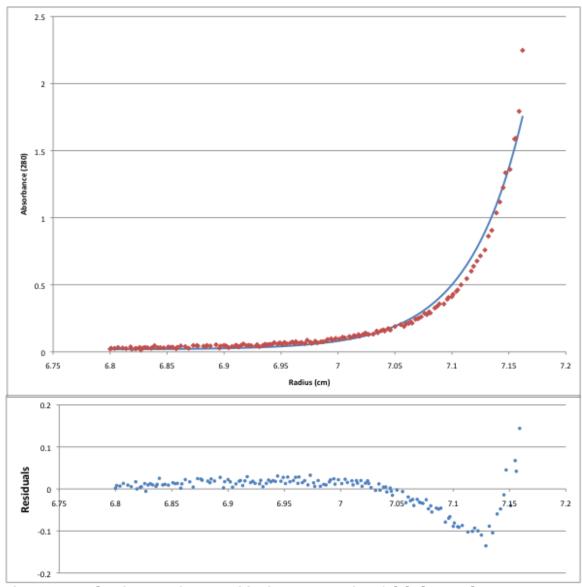**Figure 4.2: Sedimentation Equilibrium Analysis of CC-Stag.** Graph depicting absorbance profile within the ultracentrifugation cell, after reaching equilibrium at 20,000rpm. Top graph shows absorbance readings along the window fit to an exponential curve (blue line). Bottom graph shows residuals of fit line to corresponding data points. Molecular weight was determined using fit data from all three speeds.

19

CHAPTER 5

RECOMBINANT CC MAY INTERACT TRANSIENTLY WITH DYNEIN INTERMEDIATE CHAIN

Introduction

It has been previously shown that Num1 co-immunoprecipitates with Pac11, dynein's intermediate chain (Heil-Chapdelaine, 2000). *In vivo* data suggests the CC domain may be sufficient for Num1's observed interaction with the dynein complex. I performed a pull down assay to determine whether the recombinant CC domain is capable of interacting with Pac11 *in vitro.* As a positive control for the pull down I over expressed a CC-13myc construct using a Gal promoter in yeast cells.

Recombinant Protein Expression and Pull Down Protocol

To detect interaction of Pac11 or the CC domain with the coiled-coil domain, *E. Coli* BL21 Rosetta cells (Novagen) carrying pBSG02 were induced in the presence of 0.5 mM IPTG to express CC-S-ZZ at 16°C for 15-17h. Cells were harvested and lysed by bead beating for 1 minute four times. After centrifugation, the supernatant was added to 100 μl S-agarose resin (Novagen) and incubated at 4 degress for 45min with gentle rotation, followed by extensive wash with S-protein bind/wash buffer (20mM Tris-HCl pH7.5, 150mM NaCl, 1mM EDTA, 0.1% Triton X-100 1mM DTT and 1 mM phenylmethanesulfonylfluoride (PMSF)). The resins were then resuspended into UB buffer (50 mM Hepes, pH 7.5, 100 mM KCl, 3 mM MgCl, 1 mM EGTA, 1 mM DTT, 1mM PMSF and protease inhibitor

cocktail) (ref) and kept on ice. Yeast extracts were prepared from strains expressing either Pac11-13Myc or Gal::CC-13myc. Briefly, harvested cells from mid log-phase culture were washed once with distilled water and once with UB buffer, resuspended into UB buffer and then lysed by glass bead beating 4 times for 1 minute using the mini-beadbeater (Biospec). After removing cell debris by centrifugation at 4°C for 25 minutes, the supernatant was added to the resin-bound CC-S-IgG prepared above and incubated at 4°C for 30 minutes with gentle rotation. Resins were then washed with high salt UB buffer (50 mM Hepes, pH 7.5, 200 mM KCl, 3 mM MgCl, 1 mM EGTA, 1 mM DTT, 0.2% Tween-20 and1mM PMSF) for three times. Resin bound proteins were digested in 400µl UB buffer with 3.5µl PCN protease releasing CC-S and any interacting proteins. The supernatant was precipitated using chloroform/methanol. The protein pellet was then dissolved into SDS-PAGE sample buffer and analyzed by western blot.

Discussion

Analysis of the two blots reveals that while the CC domain may be capable of binding to Pac11 under low salt conditions, 100mM KCl, the interaction was not detectable above background (Figure 1A). However, when the salt concentration was increased to 200mM KCl no Pac11 bands were detectable (Figure 1B). These results indicate that there may be a weak or transient interaction between the recombinant CC and Pac11. As a positive control I was able to pull down over expressed CC-13myc using the recombinant CC (Figure 1C). Further optimization of the pull down conditions may be

required to detect the interaction between the recombinant CC and Pac11, but it is also possible that a longer construct is needed to successfully detect the interaction between Num1's CC domain and Pac11.
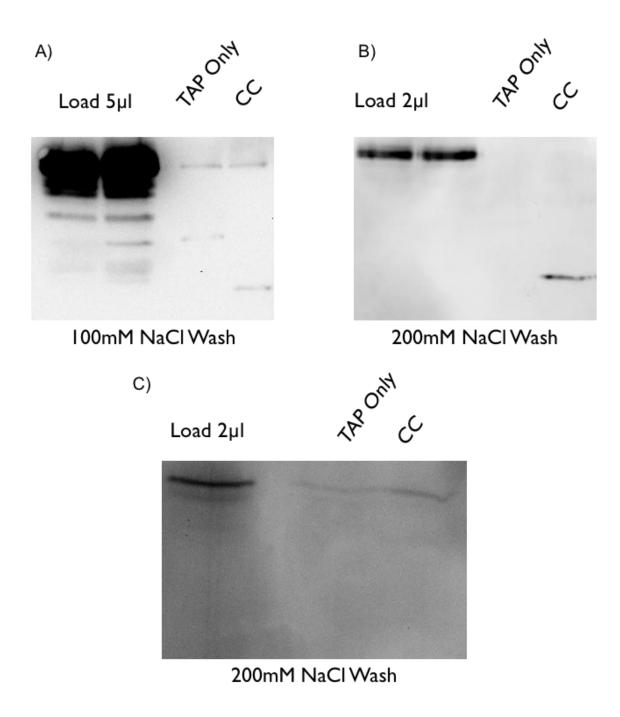
Figure 5.1: Western blot analyses of pull downs using recombinant CC.
A) Pull down of Pac11-13myc under 100mM KCl wash conditions. Binding of

Pac11-13myc was identical between recombinant CC and the vector only.
B) Pull down of Pac11-13myc under 200mM KCl wash conditions. No detectable
Pac11-13myc bands in either lane. C) Positive control for pull down using GAL
over expression of CC-13myc, cells were induced using for 3 hours using 2%
galactose.

CHAPTER 6

QUANTITATIVE ANALYSIS OF DYNEIN PATHWAY
COMPONENTS *IN VIVO*

Introduction

A recent method has been established for a quantitative ratiometric

analysis of proteins *in vivo* (Joglekar et al*.* 2006). Using Cse4, a centromeric

protein existing in two molecules per chromosome, as a standard we were able

to assay the stoichiometry of various dynein pathway components. We first

asked what was the relative ratio of dynein to its accessory chains and dynactin

at the plus-end of astral microtubules and the cortex. We then asked what was

the effect on the dynein pathway when we perturbed these ratios.

Ratiometric Quantification and Statistical Analysis

Cse4-standardized ratiometric measurements were performed as

described [Joglekar et al., 2008; Markus et al., 2009]. Strains expressing

fluorescently-tagged Cse4 or dynein pathway components were imaged using

identical imaging conditions and with 1 x 1 binning of the camera chip (Cascade

II:512). We used ImageJ to draw a circle encompassing 3 x 3 pixels to quantify

the intensity of individual Cse4, or the relevant plus end or cortical dynein

pathway foci. With a 100x magnification objective and a camera pixel size of 16

µm (Cascade II:512), each pixel corresponds to 160 nm in the object plane, a

value which we verified using a micrometer. The mean intensity of Cse4 (Figure

1) was assigned a value of 32 molecules [Meluh et al., 1998; Joglekar et al., 2006] and was used to normalize fluorescence intensity values (A.U.) to number of molecules. We used R and the model-based clustering algorithm Mclust [Fraley and Raftery, 2007] to determine whether each data set was a single normal or a mixture of multiple normal distributions, and to determine the mean and standard deviation for each component. The Mclust package for R uses an expectation-maximization algorithm to deter- mine the number of components within a given data set by maximizing the Bayesian information criterion (BIC) [Schwarz, 1978].

Discussion

Using CSE4 as a standard for fluorescence intensity and CFP-Tub1 to confirm the location of astral microtubule plus-ends, we were able to determine the relative quantities of various dynein pathway components at mobile plus-end foci, as well as stationary cortical foci. For each component we measure a high number of foci and plotted the intensity profiles and fit the data to either a single or bimodal distribution (Figure 2). Many components exhibited a second normal distribution twice the intensity of the first distribution. However, the second distribution consisted of only a small fraction of the data set, ranging from 12 to 36%. Although this remains unclear we explain the second data set as the result of overlapping microtubules. All ratio comparisons use the mean obtained from the first data set.

Analysis of the plus-end ratio of Dyn1 (dynein heavy chain) to Pac1/LIS1 revealed an apparent 1:1 ratio between Dyn1 and Pac1 foci (Figure 3). This ratio was conserved even when an inducible GAL promoter over expressed Pac1, resulting in additional Pac1/Dyn1 complexes per plus-end.

To compare the relative quantities of dynein to dynactin we measured fluorescence intensities of multiple dynactin components and found a 3:1 ratio of dynein to dynactin at the plus-ends of microtubules. We also quantified the relative fluorescence of Dyn1 to Jnm1, a component of dynactin present in 5 copies per dynactin complex, at the cortex and observed a similar 3:1 ratio. The dynein to dynactin ratio was also not affected in cells over expressing Pac1 (Figure 4).

She1 has been previously reported to be a negative regulator of dynein pathway in budding yeast (Woodruff et al. 2009). It was proposed that She1 inhibits dynactin's association with dynein at microtubule plus-ends. However, quantitative analysis of the dynein to dynactin ratio at the plus-ends has not been established in *she1Δ* cells. We also asked what affect deletion of She1 had on targeting of cortical dynein and dynactin.

In she1Δ cells we observed a change in the plus end ratio of dynein to dynactin, finding a dramatic increase in the association of dynein and dynactin on microtubule plus-ends. Using our molecule counting assay, in *she1Δ* cells, we observed an average of 9.4 ± 4.3 molecules of Dyn1 and 21.6 ± 6.0 molecules of Jnm1 at the plus-ends (Figure 4). We also quantified stationary cortical foci to observe the effect of *she1Δ* on cortical targeting of dynein and dynactin. We

found an average of 6.8 ± 3.5 molecules of Dyn1 and 12.6 ± 4.5 molecules of Jnm1 (Figure 5). Results from our molecule counting assay confirmed an increase in dynein and dynactin association in *she1Δ* cells, increasing the ratio of dynein to dynactin to 1:1 at plus-ends, as well as at the cortex. We also observed hyperactive dynein in cells expressing *she1Δ* more dramatic than values observed in Pac1 over expressing cells. This increased activity correlates with an increase in the ratio of dynactin to dynein at cortical foci. The ratio of dynein to dynactin at the plus ends was confirmed by quantification of other dynactin components, however other components could not be measured at the cortex due to low copy number in the dynactin complex. Combined with our results from over expression of Pac1 we are able to conclude that dynactin's association with dynein is not dependent on the abundance of dynein on the plus-end, rather She1 negatively regulates their association.

Previously our lab proposed that dynein's N-terminal cortical attachment domain may be "masked" inhibiting its ability to associate with cortical Num1. Our new data supports the model that dynein at the plus-ends is targeted by dynactin, which facilitates the unmasking of the N-terminal cortical attachment domain, ultimately leading to dynein off-loading on cortical Num1 foci.

In conclusion, our molecule counting assay provides a quantitative measure of relative fluorescence values, using CSE4 as a standard, to determine the relative stoichiometry of various complexes *in vivo.* Use of this technique has allowed us to expand upon our labs previous model and propose relative stoichiometry of pathway components (Figure 6).

Combined with null mutations or over expression of different pathway component molecule counting provides a relatively fast method of quantifying changes in protein stoichiometry under different regulatory conditions. Determination of relative protein stoichiometry is useful in determining regulatory functions of various components and elucidating which elements of a pathway are good candidates for further biochemical characterization.
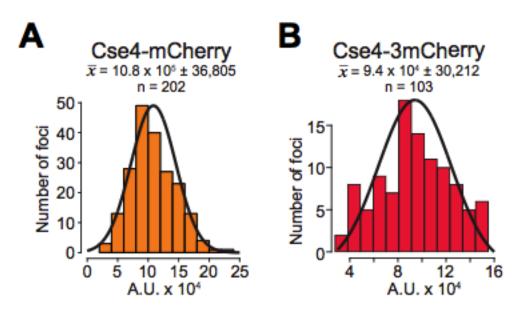

Figure 6.1: Fluorescence intensity histograms of Cse4 standards. Histograms of fluorescence intensity of individual foci of (A) Cse4-mCherry and (B) Cse4-3mCherry. Mean values from these data sets (mean ± standard deviation are shown) were used for standardizing the intensity distribution of dynein pathway components to number of molecules. Note that the differences in the fluorescence intensity values for the different Cse4 standards are due to different camera acquisition settings. Camera settings for each fluorophore (*e.g.*, 3mCherry versus mCherry) were optimized such that pixel saturation was not reached. Furthermore, Cse4 standards and the associated fluorescent dynein pathway component were imaged within no more than a week's period of each other to ensure that changes in the mercury arc lamp bulb were negligible.
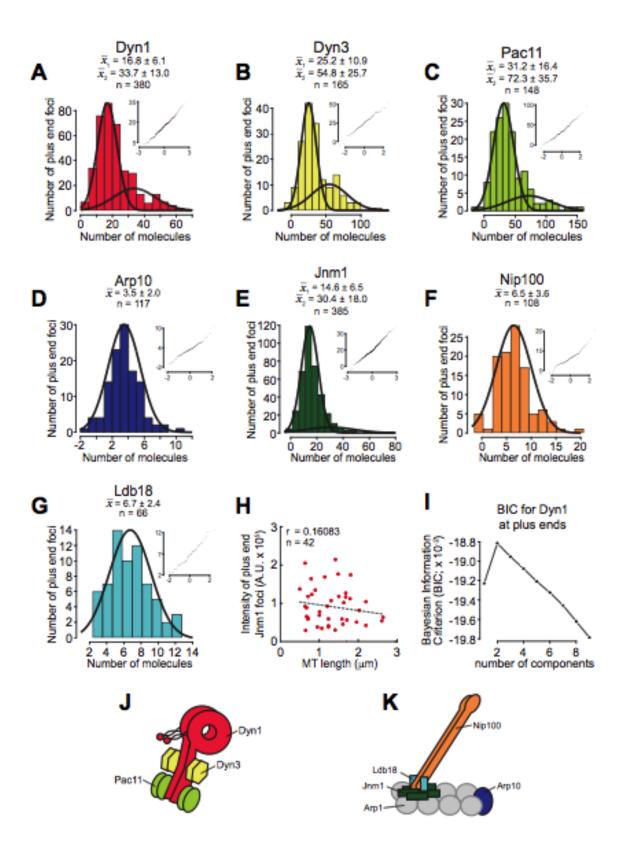
A Dyn1
$\bar{x}_1 = 16.8 \pm 6.1$
$\bar{x}_2 = 33.7 \pm 13.0$
$n = 380$

B Dyn3
$\bar{x}_1 = 25.2 \pm 10.9$
$\bar{x}_2 = 54.8 \pm 25.7$
$n = 165$

C Pac11
$\bar{x}_1 = 31.2 \pm 16.4$
$\bar{x}_2 = 72.3 \pm 35.7$
$n = 148$

D Arp10
$\bar{x} = 3.5 \pm 2.0$
$n = 117$

E Jnm1
$\bar{x}_1 = 14.6 \pm 6.5$
$\bar{x}_2 = 30.4 \pm 18.0$
$n = 385$

F Nip100
$\bar{x} = 6.5 \pm 3.6$
$n = 108$

G Ldb18
$\bar{x} = 6.7 \pm 2.4$
$n = 66$

H $r = 0.16083$
$n = 42$

I BIC for Dyn1 at plus ends

J

K

29

Figure 6.2: Quantitative ratiometric measurements of plus end associated dynein and dynactin components. Histograms of the number of molecules shown together with single or bimodal Gaussian fits (determined as described in Materials and Methods) of (A) Dyn1-3mCherry, (B) Dyn3-3mCherry, (C) Pac11-3mCherry, (D) Arp10-3mCherry, (E) Jnm1-3mCherry, (F) Nip100-3mCherry, or (G) Ldb18-3GFP per plus end focus in wild-type cells. Single or multiple normal distributions were identified using the model-based clustering algorithm Mclust, as described in Materials and Methods. Insets show quantile-quantile (Q-Q) plots with empirical quantiles on the y axis, and theoretical quantiles from a normal distribution on the x axis. For 2-component data sets, only those values probabilistically determined to occupy the first component were used for Q-Q plotting. Mean values for each component ± standard deviation are shown. (H) Plus end fluorescence intensity does not correlate with MT length (correlation coefficient, r = 0.16083). The fluorescence intensity of Jnm1-3mCherry at individual plus ends was measured and plotted against MT length. (I) An example of a Bayesian information criterion (BIC) plot from the Mclust model-based clustering algorithm. In this case, a 2-component model maximizes the BIC for the dataset of Dyn1 at plus ends shown in panel A. (J - K) Cartoon schematics depicting the *in vivo* subunit stoichiometry of the dynein and dynactin complexes at the plus end
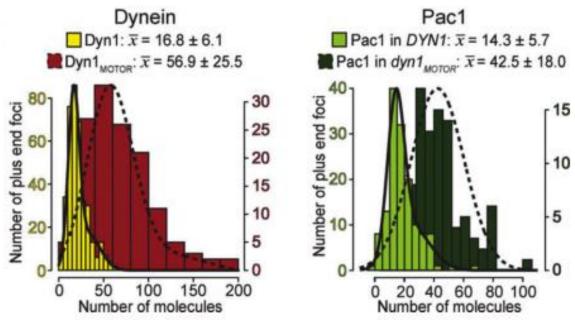

Figure 6.3: Dyn1 and Pac1 associate at plus-ends in a 1:1 ratio. Histograms of the number of molecules per plus end focus, shown together with Gaussian fits (see above for Dyn1-3mCherry (left plot, left axis; yellow; n = 380 foci), Dyn1MOTOR (left plot, right axis; red; n 5 137 foci), Pac1-3mCherry in DYN1 (right plot, left axis; light green; n = 143 foci), or Pac1-3mCherry in dyn1MOTOR-3YFP background (right plot, right axis; dark green; n = 98 foci). Mean values for each data set ± standard deviation are shown. In the case of bimodal distributions, the mean of the first major component is indicated.
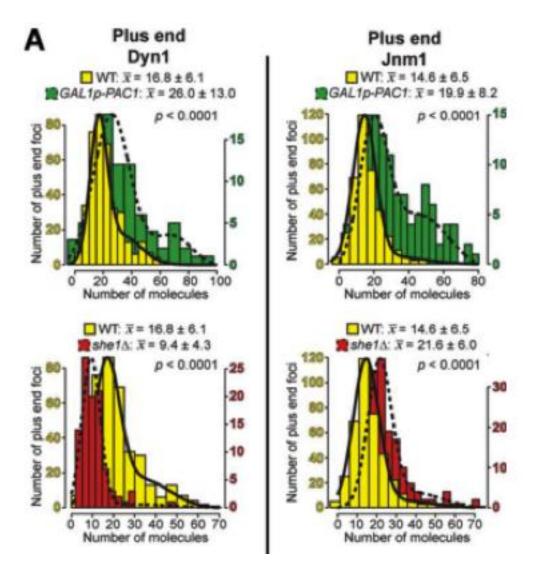
Figure 6.4: GAL1p-PAC1 and she1Δ differentially affect the recruitment of dynein and dynactin to the MT plus end. Histograms of the number of molecules per plus end focus, shown together with Gaussian fits (see "Materials and Methods") for (A) Dyn1 or Jnm1 in a wild-type (n_{Dyn1} = 380 foci; n_{Jnm1} = 385 foci), GAL1p- PAC1 (n_{Dyn1} = 80 foci; n_{Jnm1} = 124 foci), she1Δ (n_{Dyn1} = 100 foci; n_{Jnm1} = 170 foci)
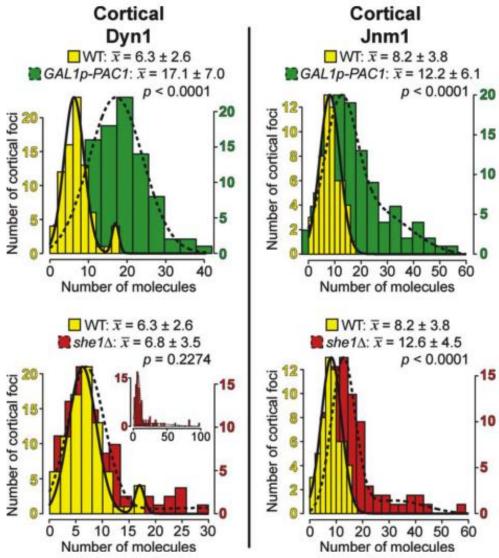
Figure 6.5: GAL1p-PAC1 and she1D differentially affect the recruitment of dynein and dynactin to the cell cortex. Histogram of the number of molecules per stationary cortical focus, shown together with Gaussian fits (see above) for Dyn1 or Jnm1 in a wild-type (n_{Dyn1} = 80 foci; n_{Jnm1} = 58 foci), GAL1p-PAC1 (n_{Dyn1} = 96 foci; n_{Jnm1} = 107 foci), or *she1Δ* strain (n_{Dyn1} = 88 foci; n_{Jnm1} = 82 foci). Mean values for the first major component ± standard deviation are shown. P values between wild-type and mutant are indicated. For 2-component data sets, only those values probabilistically determined to occupy the first component were used to calculate P values. Inset in bottom left panel depicts entire data set for cortical Dyn1 molecule number in *she1Δ* cells.
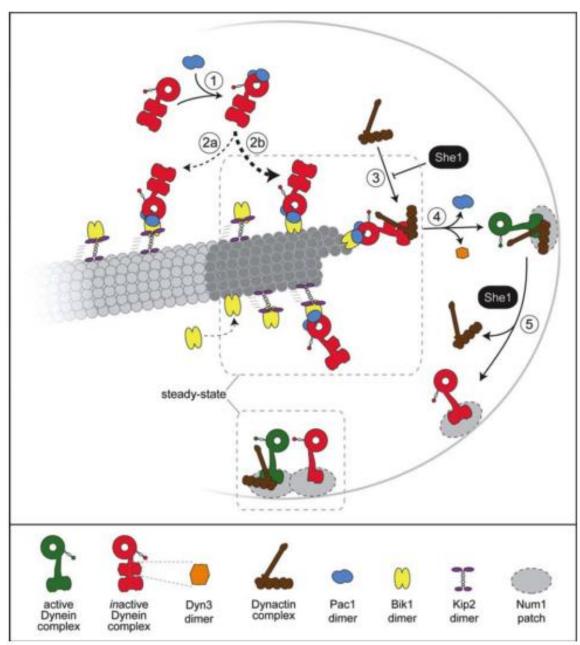
Figure 6.6: Schematic of the pathway for dynein and dynactin targeting to the plus end and cell cortex. Our data indicate that the dynein complex associates with cytoplasmic Pac1 in a 1:1 ratio (step 1) prior to interacting with plus end-bound Bik1 (step 2). Previous studies have established that Bik1/CLIP-170 is targeted to the plus end either by direct recruitment from the cytoplasm [Bieling et al., 2008; Dixit et al., 2009; Dragestein et al., 2008; Folker et al., 2005] or via a Kip2 kinesin-dependent mechanism [Carvalho et al., 2004]. Our previous data [Markus et al., 2009] showed that dynein plus end targeting is predominantly independent of Kip2 (reflected by the thickness of the dashed arrows for step 2a versus 2b). A previous study in budding yeast demonstrated that dynein then recruits dynactin to the plus end [Moore et al., 2008]. Our data here indicate that only one dynactin complex is recruited for every three plus end dynein

33

complexes. Association of dynein with dynactin (step 3), which is negatively regulated by She1 [Wood- ruff et al., 2009] (Fig. 4; Table III), is a requisite for the off-loading of dynein-dynactin to Num1 patches at the cell cortex (step 4) [Lee et al., 2003; Sheeman et al., 2003; Moore et al., 2008]. Each cortical Num1 patch consists of ~14 molecules of Num1 [Tang et al., 2009] (not all molecules are drawn). Since Pac1 and Dyn3 are not found at the cell cortex, they likely dissociate from the dynein complex during step 4 [Lee et al., 2003, 2005]. Based on our observations in this study, we propose that She1 mediates the dissociation of dynactin from cortically anchored dynein (step 5) thus maintaining a steady-state ratio of 1 dynactin per 2 dynein complexes. Our data indicate that assembled cortical dynein-dynactin complexes (green) are active, while cortical dynein without dynactin is inactive (red). Dashed gray boxes outline a diagrammatic summary of the stoichiometry our counting data has revealed for MT plus ends and the cell cortex.

REFERENCES

Beach, D.L. et al., 2000. The role of the proteins Kar9 and Myo2 in orienting the mitotic spindle of budding yeast. *Current biology : CB*, 10(23), pp.1497-506.

Bloom, K., 2001. Nuclear migration: cortical anchors for cytoplasmic dynein. *Current biology : CB*, 11(8), pp.R326-9.

Farkasovsky, M. & Küntzel, H., 2001. Cortical Num1p interacts with the dynein intermediate chain Pac11p and cytoplasmic microtubules in budding yeast. *The Journal of cell biology*, 152(2), pp.251-62.

Ghosh-Roy, A. et al., 2004. Cytoplasmic dynein-dynactin complex is required for spermatid growth but not axoneme assembly in Drosophila. *Molecular biology of the cell*, 15(5), pp.2470-83.

Gönczy, P et al., 1999. Cytoplasmic dynein is required for distinct aspects of MTOC positioning, including centrosome separation, in the one cell stage Caenorhabditis elegans embryo. *The Journal of cell biology*, 147(1), pp.135-50.

Han, G. et al., 2001. The Aspergillus cytoplasmic dynein heavy chain and NUDF localize to microtubule ends and affect microtubule dynamics. *Current biology : CB*, 11(9), pp.719-24.

Heil-Chapdelaine, R. a, Oberle, J.R. & Cooper, J a, 2000. The cortical protein Num1p is essential for dynein-dependent interactions of microtubules with the cortex. *The Journal of cell biology*, 151(6), pp.1337-44.

Joglekar, A.P. et al., 2006. Molecular architecture of a kinetochore-microtubule attachment site. *Nature cell biology*, 8(6), pp.581-5.

Lee, W.-L., Kaiser, M. a & Cooper, John a, 2005. The offloading model for dynein function: differential function of motor subunits. *The Journal of cell biology*, 168(2), pp.201-7

Mainwaring, W.I., 1969. A soluble androgen receptor in the cytoplasm of rat prostate. *The Journal of endocrinology*, 45(4), pp.531-41.

Markus, S.M., Punch, J.J. & Lee, W.-L., 2009. Motor- and tail-dependent targeting of dynein to microtubule plus ends and the cell cortex. *Current biology : CB*, 19(3), pp.196-205.

Meluh, P.B. et al., 1998. Cse4p is a component of the core centromere of
    Saccharomyces cerevisiae. *Cell*, 94(5), pp.607-13.

Tang, X., 2009 A CAAX motif can compensate for the PH domain of Num1 for
cortical dyenin attachment. *Cell cycle (Georgetown, Tex.).*

van der Voet, M. et al., 2009. NuMA-related LIN-5, ASPM-1, calmodulin and
    dynein promote meiotic spindle rotation independently of cortical LIN-
    5/GPR/Galpha. *Nature cell biology*, 11(3), pp.269-77.

Woodruff, J.B., Drubin, D.G. & Barnes, G., 2009. Dynein-Driven Mitotic Spindle
    Positioning Restricted to Anaphase by She1p Inhibition of Dynactin
    Recruitment. *Molecular Biology of the Cell*, 20(13), p.3003.